ChemPubSoc Europe

DOI: 10.1002/chem.201701480

CHEMISTRY
A European Journal
Communication

Thermoelectrics

Ultrahigh Average Thermoelectric Figure of Merit, Low Lattice Thermal Conductivity and Enhanced Microhardness in Nanostructured $(GeTe)_x(AgSbSe_2)_{100-x}$

Manisha Samanta, Subhajit Roychowdhury, Jay Ghatak, Suresh Perumal, and Kanishka Biswas*[a]

Abstract: Waste heat sources are generally diffused and provide a range of temperatures rather than a particular temperature. Thus, thermoelectric waste heat to electricity conversion requires a high average thermoelectric figure of merit (ZT_{avg}) of materials over the entire working temperature along with a high peak thermoelectric figure of merit (ZT_{max}). Herein an ultrahigh ZT_{avg} of 1.4 for $(GeTe)_{80}(AgSbSe_2)_{20}$ [TAGSSe-80, T = tellurium, A = antimony, G = germanium, S = silver, Se = selenium] is reported in the temperature range of 300–700 K, which is one of the highest values measured amongst the state-of-the-art Pb-free polycrystalline thermoelectric materials. Moreover, TAGSSe-80 exhibits a high ZT_{max} of 1.9 at 660 K, which is reversible and reproducible with respect to several heating–cooling cycles. The high thermoelectric performance of TAGSSe-*x* is attributed to extremely low lattice thermal conductivity (κ_{lat}), which mainly arises due to extensive phonon scattering by hierarchical nano/meso-structures in the TAGSSe-*x* matrix. Addition of $AgSbSe_2$ in GeTe results in κ_{lat} of $\approx 0.4\ W\,mK^{-1}$ in the 300–700 K range, approaching to the theoretical minimum limit of lattice thermal conductivity (κ_{min}) of GeTe. Additionally, $(GeTe)_{80}(AgSbSe_2)_{20}$ exhibits a higher Vickers microhardness (mechanical stability) value of $\approx 209\ kgf\,mm^{-2}$ compared to the other state-of-the-art metal chalcogenides, making it an important material for thermoelectrics.

Conversion of waste heat into useful electricity-using thermoelectric (TE) materials is a promising alternative means of power generation to consummate the global need for energy production and management.[1] Performance of TE materials is evaluated in terms of the dimensionless thermoelectric figure of merit (ZT), which is defined by $ZT = S^2\sigma T/\kappa$, where σ, S, T, and κ are the electrical conductivity, Seebeck coefficient, temperature, and total thermal conductivity of a material. Inorganic solids exhibit the maximum figure of merit (ZT_{max}) at a particular temperature, but high ZT values over a wide range of temperature, that is, a high average thermoelectric figure of merit, ZT_{avg}, are useful for thermoelectric device application. The efficiency of a thermoelectric device depends on the materials' ZT_{avg} over the entire working temperature range, rather than ZT_{max}.[2] Therefore, it is essential to improve the ZT_{avg} over the whole temperature range of interest. However, many previous strategies have focused on improving the maximum ZT as function of temperature. ZT may be enhanced through reduction of the lattice thermal conductivity (κ_{lat}) by hierarchical phonon scattering through nano/mesostructures,[3] lattice/bonding anharmonicity,[4] the effect of rattling modes,[5] and superionic substructures with liquid-like cation disordering.[6] The Seebeck coefficient of a material is enhanced either by electronic band valley convergence[7] or the formation of a resonance level in the valence band.[8] Although GeTe based alloys have been known for their promising thermoelectric properties for long time,[9] pristine GeTe was not of further interest due to its high p-type carrier concentration of $\approx 8.7\times10^{20}\ cm^{-3}$ because of the intrinsic Ge vacancies,[10] which gives rise to a high σ of $\approx 8000\ S\,cm^{-1}$, high electrical thermal conductivity (κ_{el}) and a low S of $\approx 34\ \mu V\,K^{-1}$ at room temperature.[11] The pseudo-binary solid solution compositions $(GeTe)_x(AgSbTe_2)_{100-x}$, commonly known as TAGS-*x*, are one of the traditional thermoelectric materials since their discovery in 1960.[9a,12] TAGS materials have been widely used in deep space missions by NASA for radioisotope thermoelectric generators.[12c] TAGS-85 possess a high ZT (≈ 1.5 at 750 K), low lattice thermal conductivity, and good mechanical stability.[12a] Other GeTe based materials such as $Ge_{1-x}Pb_xTe$,[13] $Ge_{1-x}(Sb/Bi)_xTe$,[14] and $(CoGe_2)_{0.22}(GeTe)_{19}Sb_2Te_3$[15] recently exhibited high ZT_{max} values at ≈ 750 K. Although most of these GeTe based materials exhibit high ZT_{max}, a high ZT over a wide range of temperature, that is, high ZT_{avg}, with good mechanical stability is desirable.

Herein, we report an ultrahigh ZT_{avg} of 1.4 between 300–700 K, along with a high ZT_{max} value of 1.9 at 660 K, in $(GeTe)_{80}(AgSbSe_2)_{20}$ which belongs to new pseudo-binary solid solution composition $(GeTe)_x(AgSbSe_2)_{100-x}$ [$x = 75$–100], termed as TAGSSe-*x* (T = tellurium, A = antimony, G = germanium, S = silver, Se = selenium, and *x* represents the percentage of GeTe). Moreover, a κ_{lat} value of $\approx 0.4\ W\,mK^{-1}$ in the 300–700 K range

[a] M. Samanta, S. Roychowdhury, Dr. J. Ghatak, Dr. S. Perumal, Dr. K. Biswas
New Chemistry Unit & International Center for Materials Science
Jawaharlal Nehru Centre for Advanced Scientific Research (JNCASR)
Jakkur, Bangalore (India)
E-mail: kanishka@jncasr.ac.in
Homepage: http://www.jncasr.ac.in/kanishka/

Supporting information and the ORCID identification number(s) for the author(s) of this article can be found under https://doi.org/10.1002/chem.201701480.

was achieved for TAGSSe-80, which is close to the theoretical minimum limit (κ_{min}) of GeTe. This is the lowest κ_{lat} value measured so far among GeTe based materials. Transmission electron microscopy (TEM) reveals the formation of hierarchical nano/mesostructures of different dimensions and compositions in the GeTe matrix, which provide significant phonon scattering of different wavelengths to result in the ultralow κ_{lat} in TAGSSe-*x*. Additionally, TAGSSe-80 exhibits a high Vickers microhardness (H_v) (mechanical stability) value of $\approx$209 kgf mm^{-2}, which is higher than that of the state-of-the-art metal chalcogenide based thermoelectric materials.

Pristine GeTe exhibits a κ_{lat} of $\approx$2.7 W mK^{-1} at room temperature,[14a] whereas the theoretical limit of minimum lattice thermal conductivity (κ_{min}) of GeTe is $\approx$0.3 W mK^{-1}. This hints that there is enormous scope to decrease the κ_{lat} of GeTe. To minimize the κ_{lat} of GeTe, we have particularly chosen the combination of GeTe and $AgSbSe_2$, considering the fact that $AgSbSe_2$ has an ultralow κ_{lat} of $\approx$0.35 W mK^{-1} in the 300–700 K range due to Sb lone pair induced bond anharmonicity.[4c] Furthermore, the addition of $AgSbSe_2$ into GeTe may result in the formation of second phase nanostructures in the GeTe matrix, due to lattice parameter mismatch of GeTe and $AgSbSe_2$, which may result in a low κ_{lat} in GeTe. With this motivation, we have synthesized different GeTe-rich compositions of TAGSSe-*x* crystalline ingots and studied the structural, microscopic, and thermoelectric properties in detail.

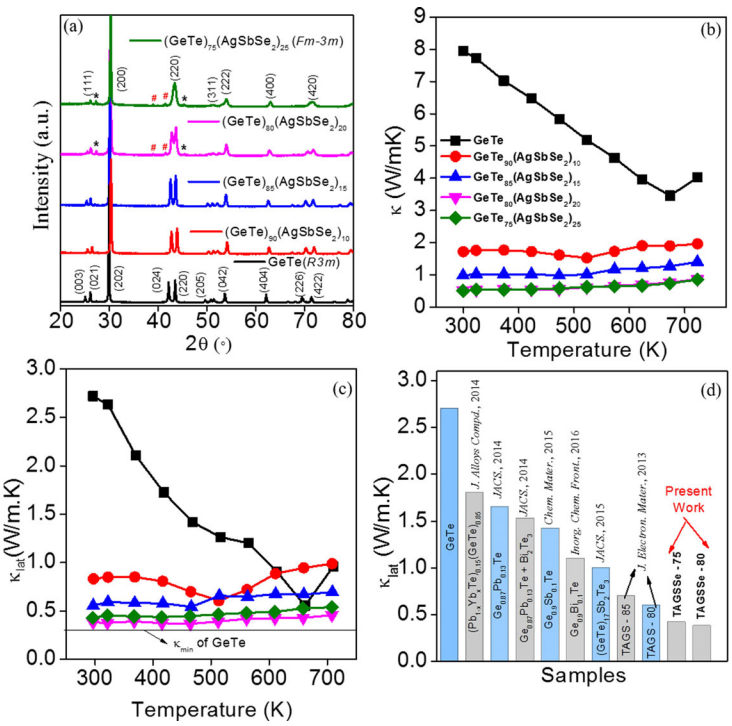

Figure 1. (a) Powder XRD pattern of $(GeTe)_x(AgSbSe_2)_{100-x}$ (x=75–100). "*" and "#" signs indicate the presence of Ge- and $Ag_{4.53}Te_3$-rich second phases, respectively. Temperature dependent (b) thermal conductivity (κ) and (c) lattice thermal conductivity (κ_{lat}) of TAGSSe-*x* (x=75–100) samples. (d) Histogram showing κ_{lat} for TAGSSe-*x* (x=80, 75) and different GeTe-based thermoelectric materials.

The powder X-ray diffraction (PXRD) patterns of TAGSSe-*x* (x=75–100) at room temperature are presented in Figure 1a. All samples except TAGSSe-75 could be indexed based on the rhombohedral structure of GeTe (space group *R*3*m*), whereas TAGSSe-75 could be indexed based on cubic structure of GeTe (space group $Fm\bar{3}m$) (Figure 1a, Figures S1 and S2 in Supporting Information). With the increase in the percentage of $AgSbSe_2$ in TAGSSe-*x*, the double peaks of (0 2 4) and (2 2 0) between 2θ=41–45° approach closer and ultimately converge to a single peak for $(GeTe)_{75}(AgSbSe_2)_{25}$, suggesting that the cubic nature of the samples increases with the increase in $AgSbSe_2$ concentration. In the PXRD patterns of $(GeTe)_x(AgSbSe_2)_{100-x}$, additional reflections due to second phases are also observed for x=75 and 80. These low intensity reflections occur due to the existence of second phases of Ge (space group, $Fd\bar{3}m$) and of $Ag_{4.53}Te_3$ (space group, $P\bar{6}2m$) (Figure 1a).

Figure 1b shows the temperature dependent total thermal conductivity (κ_{total}) of TAGSSe-*x* (x=75–100) samples. A significant reduction of κ_{total} is observed with increasing $AgSbSe_2$ in TAGSSe-*x*. At room temperature, GeTe exhibits a κ_{total} of $\approx$8 W mK^{-1}, which is suppressed to a value of $\approx$0.51 W mK^{-1} in TAGSSe-75, which is the lowest κ_{total} value measured among all the GeTe based thermoelectric materials. For $(GeTe)_x(AgSbSe_2)_{100-x}$ (x=90, 85), the temperature dependent κ_{total} shows an anomaly at $\approx$525 K, which is due the structural phase transition (rhombohedral to cubic) of GeTe. The transition temperature is significantly decreased in TAGSSe compared to pristine GeTe ($\approx$700 K). The electronic thermal conductivity (κ_{el}) of TAGSSe samples (Figure S3 in Supporting Information) is estimated from the Wiedemann–Franz law, $\kappa_{el}=L\sigma T$, where L is the Lorenz number and σ is the electrical conductivity at temperature, T. The temperature dependent Lorenz number was calculated based on the fitting of the temperature dependence of the Seebeck values (Figure S4, Supporting Information) assuming a single parabolic band model.[3a] Lattice thermal conductivities (κ_{lat}) of the all samples are shown in Figure 1c, which were obtained by subtracting κ_{el} from κ_{total}. κ_{lat} for all the samples is decreased significantly compared to that of the pristine GeTe samples. $(GeTe)_{80}(AgSbSe_2)_{20}$ exhibits a κ_{lat} of $\approx$0.4 W mK^{-1} at 300 K, which remains nearly flat throughout the measured temperature range (Figure 1c). The κ_{lat} of TAGSSe-80 is ultralow and approaching close to the theoretical minimum limit of thermal conductivity (κ_{min}) of $\approx$0.3 W mK^{-1} in GeTe, which has been calculated using Cahill's formulation [Eq. (1)]:[16a]

$$\kappa_{min} = \frac{1}{2}\left(\frac{\pi}{6}\right)^{1/3} k_B V^{-2/3} (2\nu_t + \nu_l) \quad (1)$$

where k_B is the Boltzmann constant, V is the average volume per atom, ν_t and ν_l are the transverse and longitudinal sound velocities. The average sound velocity (ν_m) and Poisson ratio (P) are directly related to ν_l and ν_t by Equation (2):[16b]

$$\nu_m = \left[\frac{1}{3}\left(\frac{2}{\nu_t^3}+\frac{1}{\nu_l^3}\right)\right]^{-1/3};\ P = \frac{1-2\left(\frac{\nu_t}{\nu_l}\right)^2}{2-2\left(\frac{\nu_t}{\nu_l}\right)^2} \quad (2)$$

By using values of $\nu_m \approx 1900\ m\,S^{-1}$[16c] and $P \approx 0.24$ from GeTe,[12b] ν_l and ν_t were calculated using the above two equations. In Figure 1d, we compared the κ_{lat} of the present TAGSSe samples with other state-of-the-art GeTe-based thermoelectric materials[12a,13b,14,15a,16d] and found that the κ_{lat} of TAGSSe-75 and TAGSSe-80 are the lowest amongst them.

In order to understand the origin of the observed ultralow κ_{lat} of $(GeTe)_x(AgSbSe_2)_{100-x}$ ($x = 80$, 75), we have performed a detailed transmission electron microscopy (TEM) study. $(GeTe)_{80}(AgSbSe_2)_{20}$ and $(GeTe)_{75}(AgSbSe_2)_{25}$ both undergo phase-separation, leading to the formation of hierarchical nano/mesostructures which cause extensive scattering of heat carrying phonons of different wavelengths. Figure 2 and Figure 3 depict the observed nano/mesostructures of TAGSSe-80 and TAGSSe-75, respectively. Low magnification TEM images of TAGSSe-80 illustrate the formation of different phase-separated nanoprecipitates of irregular sizes and mesoscale grains (Figure 2a). The corresponding high resolution TEM (HRTEM) image (highlighted area of Figure 2a) given in Figure 2b represents a crystalline nanoprecipitate, with relatively darker contrast, situated near the grain boundary. Another low-magnification TEM image of TAGSSe-80 and representative HRTEM of one of the dark contrast nanoprecipitates (highlighted in Figure 2c) are presented in Figure 2c and d, respectively. The calculated d-spacing of both the dark contrast precipitates (obtained from the HRTEM images in Figure 2b and d) is found to be 0.305 nm, which is best attributed to the (2 1 4) planes of $Ag_{4.53}Te_3$ phase (space group $P\bar{6}2m$).[17] This finding is further supported by the observation of $Ag_{4.53}Te_3$ phase as a low intensity second phase in the PXRD patterns (Figure 1a). In order to find out the composition of different nanoprecipitates, energy dispersive X-ray analysis (EDAX) was performed (Figure 2e). Nanoprecipitates of relatively darker contrast consist of AgTe-rich phases, whereas precipitates of lighter contrast are Ge-rich phases (Figure 2e). We could not quantitatively determine the exact composition of individual nanoprecipitates by EDAX analysis, as these nanoprecipitates overlap with the matrix as well as with other nanoprecipitates. Observed additional low intensity reflections in the PXRD pattern due to Ge and $Ag_{4.53}Te_3$ phases (Figure 1a) further supports the findings of the EDAX analysis. Figure 2f shows an HRTEM image of TAGSSe-80 consisting of very small (2–6 nm) nanodots of Ag_2Te (space group, $P2_1/c$), which is more prominent in the case of the TAGSSe-75 sample (discussed later).

Figure 3a represents a low magnification TEM image of TAGSSe-75, which shows presence of dark contrast precipitates

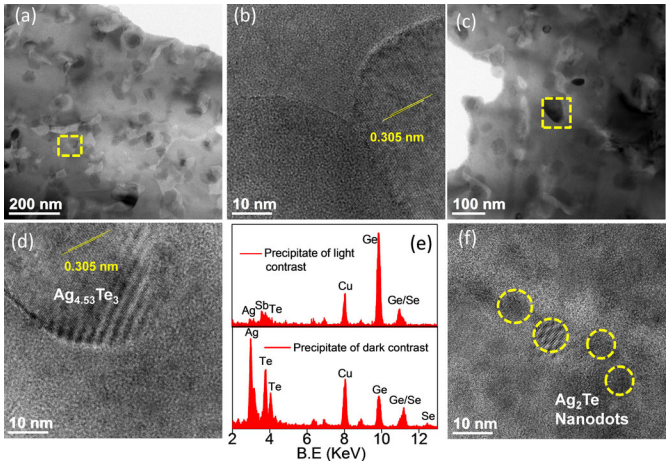

Figure 2. (a) Low magnification TEM image of $(GeTe)_{80}(AgSbSe_2)_{20}$, (b) HRTEM of the highlighted area of (a). (c) Low magnification TEM image of $(GeTe)_{80}(AgSbSe_2)_{20}$, (d) HRTEM of the black precipitate, highlighted in (c). (e) EDAX of the dark and light contrast nanoprecipitates. (f) HRTEM image of $(GeTe)_{80}(AgSbSe_2)_{20}$, from another region, showing the presence of Ag_2Te nanodots.

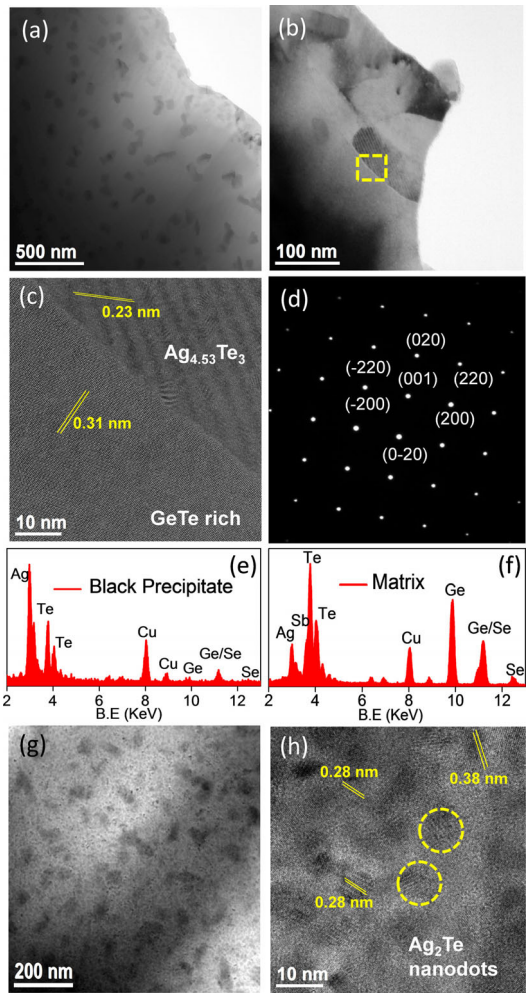

Figure 3. (a) Low magnification TEM image of $(GeTe)_{75}(AgSbSe_2)_{25}$, (b) zoomed TEM image of the nanoprecipitate indicated in (a). (c) HRTEM of the highlighted area of (b). (d) SAED pattern of the matrix region along the $<0\,0\,1>$ zone axis. (e),(f) EDAX of the precipitate and matrix, respectively from (c). (g) Low magnification TEM image of another typical region of $(GeTe)_{75}(AgSbSe_2)_{25}$, (h) HRTEM showing presence of small Ag_2Te nanodots with corresponding lattice spacing.

of irregular sizes in the range 20–80 nm distributed uniformly in the GeTe matrix. The zoomed TEM image of the nanoprecipiate and HRTEM image of that nanoprecipiate (highlighted in Figure 3b) are shown in Figure 3b and c, respectively. The HRTEM image shows a lattice spacing of the matrix of 0.31 nm which corresponds to the (200) planes of cubic GeTe, whereas a d-spacing of 0.23 nm of the precipitate is best attributed to (500) planes of $Ag_{4.53}Te_3$ (space group, $P\bar{6}2m$). The measured PXRD pattern of TAGSSe-75 further corroborates the observed findings (Figure 1a). The selected area diffraction pattern (SAED) obtained from the matrix (Figure 3d) further confirms the occurrence of the cubic phase of GeTe when the concentration of $AgSbSe_2$ in the alloy is as high as 25%. In order to understand the composition, EDAX has been performed on both the matrix and the precipitate (Figure 3e and f). While the matrix is cubic $Ge_{1-x}Sb_xTe_{1-y}Se_y$, the darker contrast nanoprecipitates (20–80 nm) are $Ag_{4.53}Te_3$-rich phases. Figure 3g and h show low magnification TEM images and the corresponding HRTEM image of TAGSSe-75 from a different region, which illustrate the presence of numerous small nanodots (2–6 nm). Calculation of the d-spacing of the nanodots confirms the presence of the Ag_2Te phase (space group, $P2_1/c$). The measured d-spacing of the nanodots is 0.28 nm which is best attributed to the (−212) planes of Ag_2Te, having the highest intensity of reflection in the PXRD, whereas a d-spacing of 0.38 nm corresponds to the (011) planes of Ag_2Te. The presence of nanoscale dots/precipitates along with mesoscale grain boundaries gives rise to hierarchical nano/mesostructuring in TAGSSe in different length scales, which causes significant scattering of heat carrying phonons of different wavelengths, thereby resulting in the ultralow lattice thermal conductivity in TAGSSe-*x* ($x = 80$, 75).

The carrier concentration (n) of all the TAGSSe-*x* ($x = 75$–100) samples were estimated using the formula $n = 1/(eR_H)$; where e is the electronic charge and R_H is the Hall coefficient. R_H values, measured at room temperature for all the samples, were found to be positive, indicating p-type carriers (see Table S1 in the Supporting Information). The p-type carrier concentrations decrease from 8.72×10^{20} cm^{-3} in pristine GeTe to 2.6×10^{19} cm^{-3} in TAGSSe-75. STEM-EDAX indicates that the matrix is Sb-doped $GeTe_{1-y}Se_y$, therefore Sb^{3+} dopes into the Ge^{2+} sublattice. This introduces an extra electron,[14] which indeed decreases the p-type carrier concentration in TAGSSe-*x* compared to that of pristine GeTe. Previous electronic structure calculations also predicted the donor dopant nature of Sb in GeTe.[14c]

The temperature dependent electrical conductivity (σ) of all the TAGSSe-*x* ($x = 75$–100) samples, measured in the range of 300–723 K, are presented in Figure 4a. Alloying of $AgSbSe_2$ with GeTe suppresses the carrier concentration because of the donor dopant nature of Sb,[14c] thereby decreasing the σ according to the equation, $\sigma = ne\mu$ (μ = mobility of the carrier). GeTe has a very high σ of ≈7584 S cm^{-1} at room temperature due to high carrier concentration, which decreases to ≈2329 S cm^{-1} at 710 K, indicating a degenerate semiconductor behavior. The room temperature σ of TAGSSe-90 is ≈1408 S cm^{-1}, which decreases to ≈170 S cm^{-1} for TAGSSe-75

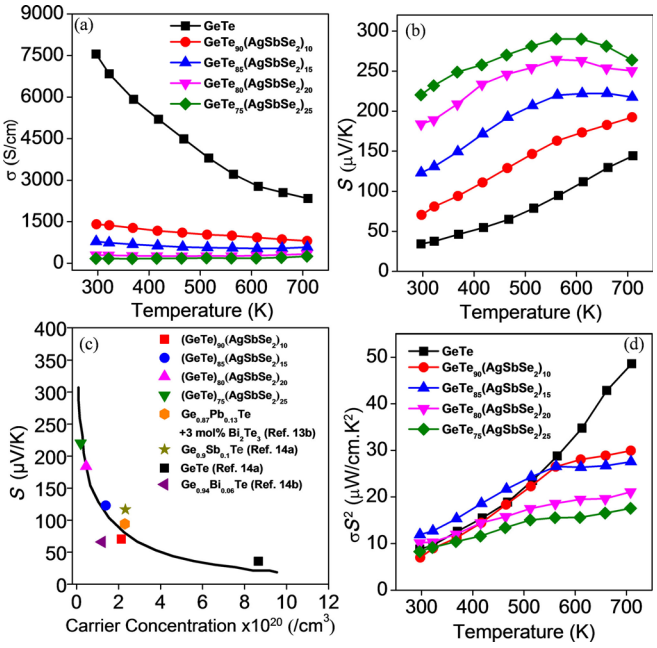

Figure 4. Temperature dependent (a) electrical conductivity (σ), (b) Seebeck coefficient (S), and (d) power factor (σS^2) of $(GeTe)_x(AgSbSe_2)_{100-x}$ ($x = 100$–75) samples. (c) S vs. n data for $(GeTe)_x(AgSbSe_2)_{100-x}$ ($x = 100$–75) samples along with previously reported S vs. n of other GeTe based samples and Pisarenko plot[13b] of GeTe at room temperature.

as we increase the concentration of $AgSbSe_2$ in TAGSSe-*x* (Figure 4a).

In Figure 4b, the temperature dependent Seebeck coefficients (S) of the TAGSSe-*x* ($x = 75$–100) are presented, which are positive for all the samples, indicating p-type conduction. A significant increase in the Seebeck coefficient is observed with an increase in the $AgSbSe_2$ concentration in GeTe. Typically S increases from ≈34 μV K^{-1} in GeTe to ≈248 μV K^{-1} for TAGSSe-75 at 300 K, which reaches up to ≈264 μV K^{-1} at 709 K for TAGSSe-75. In order to understand the mechanism of the significant increase of S in TAGSSe-*x*, we compared S versus n data for different TAGSSe-*x* samples with the previously reported Pisarenko plot for GeTe[13b] and S versus n of different GeTe based samples[13b,14] at room temperature (see Figure 4c). All the points corresponding to the present TAGSSe-*x* samples fall on or close to the Pisarenko curve of GeTe, suggesting the increase in S is solely due to the decrease in p-type carrier concentration (see Table S1 in Supporting Information).

The temperature dependent power factor (σS^2) of all the TAGSSe-*x* ($x = 75$–100) samples are shown in Figure 4d. TAGSSe-85 has a σS^2 of ≈12 μW cm^{-1}K^{-2} at room temperature which rises upto ≈28 μW cm^{-1}K^{-2} at 708 K, whereas TAGSSe-90 has σS^2 of ≈7 μW cm^{-1}K^{-2} at room temperature which reaches to high value of ≈30 μW cm^{-1}K^{-2} at 710 K. It should be mentioned that all TAGSSe-*x* samples exhibit a lower σS^2 compared to pristine GeTe at higher temperatures due to a significant decrease in the σ. In terms of overall thermoelectric performance TAGSSe-*x* gains over GeTe due to significant reduction of thermal conductivity.

The temperature dependent ZT of all the TAGSSe-*x* ($x = 75$–100) samples are illustrated in Figure 5a. As a result of ultralow

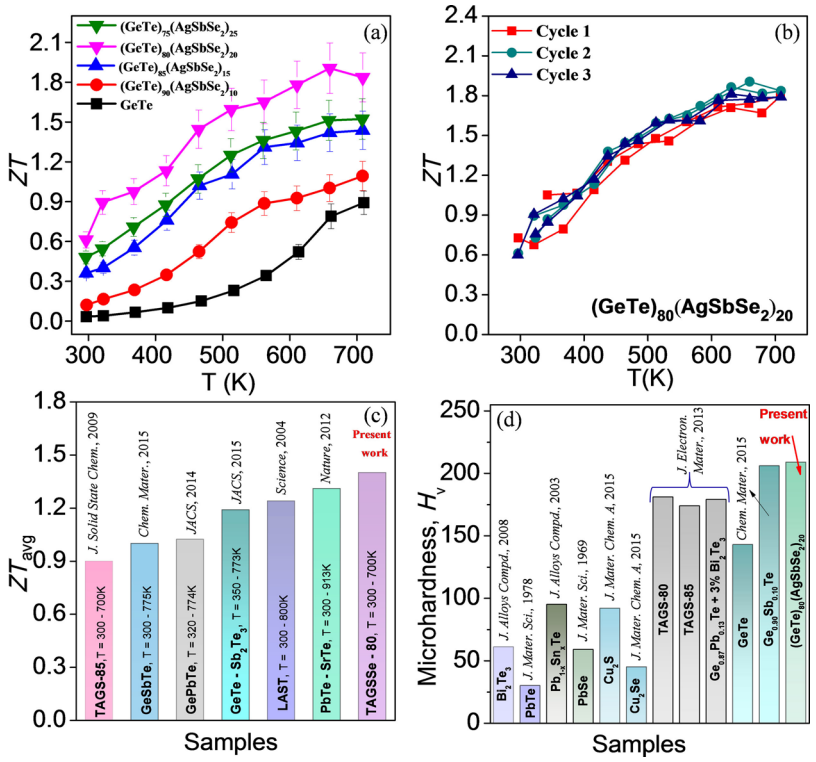

Figure 5. (a) Temperature dependent figure of merit (ZT) of TAGSSe-x ($x = 75$–100) samples. (b) Three cycles heating–cooling ZT vs. T data of TAGSSe-80. (c) Comparison of ZT_{avg} of TAGSSe-80 with other bulk state-of-the-art materials. (d) Vickers microhardness value (H_v) of GeTe and $(GeTe)_{80}(AgSbSe_2)_{20}$ along with other metal chalcogenides.

thermal conductivity, ZT_{max} reaches the highest value of 1.9 at 660 K for TAGSSe-80. TAGSSe-75 and TAGSSe-85 also exhibit a high ZT_{max} of 1.5 and 1.43 at 710 K, respectively. Three-cycle heating–cooling data of ZT versus T for $(GeTe)_{80}(AgSbSe_2)_{20}$ reveals the temperature stability and reversibility of the high ZT (see Figure 5b).

To implement the thermoelectric technology commercially, thermoelectric materials should have a high efficiency, which is directly related to ZT_{avg} of a material.[2] This is essential because the temperature of heat sources ranges from medium to high, without having a fixed temperature. Thus, a thermoelectric material must have a high ZT_{avg} over the entire working temperature range in addition to a high ZT_{max} at a particular temperature. TAGSSe-80 has a ZT of 0.6 at 300 K and 1.9 at 660 K respectively. As a result, TAGSSe-80 exhibits a high ZT_{avg} of 1.4 in the temperature range of 300–700 K. Although $PbTe_{0.7}S_{0.3}$ exhibits a high ZT_{avg} value,[2,4a] the present TAGSSe-80 exhibits one of the highest ZT_{avg} values amongst all the state-of-the-art Pb-free polycrystalline thermoelectric materials. Figure 5c is a histogram showing the ZT_{avg} of $(GeTe)_{80}(AgSbSe_2)_{20}$ along with different state-of-the-art thermoelectric materials.[3a,12b,13b,14a,15a,18]

A thermoelectric material should have good mechanical stability, but it is rare for metal chalcogenides. The measured Vickers microhardness (H_v) for TAGSSe-80 is $\approx$209 kgf mm^{-2}, whereas pristine GeTe and $AgSbSe_2$ have H_v values of $\approx$143 and $\approx$183 kgf mm^{-2}, respectively. We have compared the H_v value of TAGSSe-80 with different state-of-the-art metal chalcogenide based thermoelectric materials in Figure 5d.[12a,19] TAGSSe-x exhibit the highest Vickers microhardness values amongst all the state-of-the-art metal chalcogenide thermoelectric materials.

In conclusion, alloying of GeTe with $AgSbSe_2$ leads to an ultralow κ_{lat} of $\approx$0.4 W mK^{-1} for TAGSSe-80 in the 300–700 K temperature range, which is approaching the κ_{min} ($\approx$0.3 W mK^{-1}) in GeTe. Detailed transmission electron microscopy studies reveal that both the TAGSSe-80 and TAGSSe-75 samples exhibit all-scale hierarchical architectures starting from mesoscale grain boundaries to nanoscale precipitates to nanodots, which in turn lead to the significant scattering of heat carrying phonons of different wavelengths. Such an ultralow thermal conductivity leads to a high figure of merit, ZT, of 1.9 at 660 K for TAGSSe-80. More interestingly, an ultrahigh ZT_{avg} of 1.4 for TAGSSe-80 is obtained in the temperature range 300–700 K, which provides another dimension of importance to this material. In addition to that, this material possesses a high mechanical stability compared to other premier metal chalcogenide thermoelectric materials, making it desirable for thermoelectric exploration and further studies.

Acknowledgements

This work was supported by Ramanujan Fellowship, DST; SERB (EMR/2016/000651) and Sheik Saqr Laboratory. M.S. and S.R thank UGC and CSIR for research fellowships, respectively.

Conflict of interest

The authors declare no conflict of interest.

Keywords: chalcogenides · mechanical stability · nanostructures · thermal conductivity · thermoelectric

[1] a) J. Sootsman, D. Y. Chung, M. G. Kanatzidis, *Angew. Chem. Int. Ed.* **2009**, *48*, 8616; *Angew. Chem.* **2009**, *121*, 8768; b) H. S. Kim, W. Liu, G. Chen, C.-W. Chu, Z. Ren, *Proc. Natl. Acad. Sci. USA* **2015**, *112*, 8205; c) G. Tan, L. D. Zhao, M. G. Kanatzidis, *Chem. Rev.* **2016**, *116*, 12123 – 12149.

[2] H. J. Wu, L.-D. Zhao, F. S. Zheng, D. Wu, Y. L. Pei, X. Tong, M. G. Kanatzidis, J. Q. He, *Nat. Commun.* **2014**, *5*, 4515.

[3] a) K. Biswas, J. He, Q. Zhang, G. Wang, C. Uher, V. P. Dravid, M. G. Kanatzidis, *Nat. Chem.* **2011**, *3*, 160 – 166; b) K. Biswas, J. He, I. D. Blum, C. I. Wu, T. P. Hogan, D. N. Seidman, V. P. Dravid, M. G. Kanatzidis, *Nature* **2012**, *489*, 414 – 418; c) B. Poudel, Q. Hao, Y. Ma, Y. Lan, A. Minnich, B. Yu, X. Yan, D. Wang, A. Muto, D. Vashaee, X. Chen, J. Liu, M. S. Dresselhaus, G. Chen, Z. Ren, *Science* **2008**, *320*, 634 – 638; d) A. Banik, B. Vishal, S. Perumal, R. Datta, K. Biswas, *Energy Environ. Sci.* **2016**, *9*, 2011 – 2019.

[4] a) L. D. Zhao, G. Tan, S. Hao, J. He, Y. Pei, H. Chi, H. Wang, S. Gong, H. Xu, V. P. Dravid, C. Uher, G. J. Snyder, C. Wolverton, M. G. Kanatzidis, *Science* **2016**, *351*, 141 – 144; b) D. T. Morelli, V. Jovovic, J. P. Heremans, *Phys. Rev. Lett.* **2008**, *101*, 035901; c) S. N. Guin, A. Chatterjee, D. S. Negi, R. Datta, K. Biswas, *Energy Environ. Sci.* **2013**, *6*, 2603 – 2608.

[5] a) M. K. Jana, K. Pal, U. V. Waghmare, K. Biswas, *Angew. Chem. Int. Ed.* **2016**, *55*, 7792 – 7796; *Angew. Chem.* **2016**, *128*, 7923 – 7927; b) X. Shi, J. Yang, J. R. Salvador, M. Chi, J. Y. Cho, H. Wang, S. Bai, J. Yang, W. Zhang, L. Chen, *J. Am. Chem. Soc.* **2011**, *133*, 7837 – 7846.

[6] H. Liu, X. Shi, F. Xu, L. Zhang, W. Zhang, L. Chen, Q. Li, C. Uher, T. Day, G. J. Snyder, *Nat. Mater.* **2012**, *11*, 422 – 425.

[7] a) Y. Pei, X. Shi, A. LaLonde, H. Wang, L. Chen, G. J. Snyder, *Nature* **2011**, *473*, 66 – 69; b) W. Liu, X. Tan, K. Yin, H. Liu, X. Tang, J. Shi, Q. Zhang, C. Uher, *Phys. Rev. Lett.* **2012**, *108*, 166601.

[8] a) A. Banik, U. S. Shenoy, S. Saha, U. V. Waghmare, K. Biswas, *J. Am. Chem. Soc.* **2016**, *138*, 13068 – 13075; b) J. P. Heremans, V. Jovovic, E. S. Toberer, A. Saramat, K. Kurosaki, A. Charoenphakdee, S. Yamanaka, G. J. Snyder, *Science* **2008**, *321*, 554 – 557; c) Q. Zhang, B. Liao, Y. Lan, K. Lukas, W. Liu, K. Esfarjani, C. Opeil, D. Broido, G. Chen, Z. Ren, *Proc. Natl. Acad. Sci. USA* **2013**, *110*, 13261 – 13266.

[9] a) F. D. Rosi, J. P. Dismukes, E. F. Hockings, *Electr. Eng.* **1960**, *79*, 450 – 459; b) S. Perumal, S. Roychowdhury, K. Biswas, *J. Mater. Chem. C* **2016**, *4*, 7520 – 7536.

[10] a) T. A. Christakudi, S. K. Plachkova, G. C. Christakudis, *Phys. Status Solidi A* **1995**, *147*, 211 – 220; b) J. E. Lewis, *Phys. Status Solid A* **1970**, *38*, 131 – 140; c) D. H. Damon, M. S. Lubell, R. Mazelsky, *J. Phys. Chem. Solids* **1967**, *28*, 520 – 522.

[11] E. M. Levin, M. F. Besser, R. Hanus, *J. Appl. Phys.* **2013**, *114*, 083713.

[12] a) J. Davidow, Y. Gelbstein, *J. Eelectron. Mater.* **2013**, *42*, 1542 – 1549; b) J. R. Salvador, J. Yang, X. Shi, H. Wang, A. Wereszczak, *J. Solid State Chem.* **2009**, *182*, 2088 – 2095; c) Y. Chen, C. M. Jaworski, Y. B. Gao, H. Wang, T. J. Zhu, G. J. Snyder, J. P. Heremans, X. B. Zhao, *New J. Phys.* **2014**, *16*, 013057.

[13] a) Y. Gelbstein, J. Davidow, S. N. Girard, D. Y. Chung, M. G. Kanatzidis, *Adv. Energy Mater.* **2013**, *3*, 815 – 820; b) D. Wu, L.-D. Zhao, S. Hao, Q. Jiang, F. Zheng, J. W. Doak, H. Wu, H. Chi, Y. Gelbstein, C. Uher, C. Wolverton, M. G. Kanatzidis, J. He, *J. Am. Chem. Soc.* **2014**, *136*, 11412 – 11419.

[14] a) S. Perumal, S. Roychowdhury, D. S. Negi, R. Datta, K. Biswas, *Chem. Mater.* **2015**, *27*, 7171 – 7178; b) S. Perumal, S. Roychowdhury, K. Biswas, *Inorg. Chem. Front.* **2016**, *3*, 125 – 132; c) K. Hoang, S. D. Mahanti, M. G. Kanatzidis, *Phys. Rev. B* **2010**, *81*, 115106.

[15] a) F. Fahrnbauer, D. Souchay, G. Wagner, O. Oeckler, *J. Am. Chem. Soc.* **2015**, *137*, 12633 – 12638; b) T. Rosenthal, M. N. Schneider, C. Stiewe, M. Doblinger, O. Oeckler, *Chem. Mater.* **2011**, *23*, 4349 – 4356.

[16] a) D. Cahill, S. Watson, R. Pohl, *Phys. Rev. B* **1992**, *46*, 6131 – 6140; b) Y. Pei, J. He, J.-F. Li, F. Li, Q. Liu, W. Pan, C. Barreteau, D. Berardan, N. Dragoe, L. D. Zhao, *NPG Asia Mater.* **2013**, *5*, e47; c) P. Bauer Pereira, I. Sergueev, S. Gorsse, J. Dadda, E. Muller, J. P. Hermann, *Phys. Status Solidi B* **2013**, *250*, 1300 – 1307; d) J. F. Deng, J. Q. Li, R. F. Ye, X. Y. Liu, S. Liu, W. Q. Ao, *J. Alloys Compd.* **2014**, *585*, 173 – 177.

[17] J. Peters, O. Conrad, B. Bremer, B. Krebs, *Z. Anorg. Allg. Chem.* **1996**, *622*, 1823 – 1832.

[18] K. F. Hsu, S. Loo, F. Guo, W. Chen, J. S. Dyck, C. Uher, T. Hogan, E. K. Polychroniadis, M. G. Kanatzidis, *Science* **2004**, *303*, 818 – 821.

[19] a) L. D. Zhao, B.-P. Zhang, J.-F. Li, M. Zhou, W.-S. Liu, J. Liu, *J. Alloys Compd.* **2008**, *455*, 259 – 264; b) Y. Gelbstein, G. Gotesman, Y. Lishzinker, Z. Dashevsky, M. P. Dariel, *Scr. Mater.* **2008**, *58*, 251 – 254; c) A. J. Crocker, M. Wilson, *J. Mater. Sci.* **1978**, *13*, 833 – 842; d) J. L. Cui, X. Qian, X. B. Zhao, *J. Alloys Compd.* **2003**, *358*, 228 – 234; e) M. S. Darrow, W. B. White, R. Roy, *J. Mater. Sci.* **1969**, *4*, 313 – 319; f) L. Zhao, X. Wang, F. Y. Fei, J. Wang, Z. Cheng, S. Dou, J. Wanga, G. J. Snyder, *J. Mater. Chem. A* **2015**, *3*, 9432 – 9437.

Manuscript received: April 4, 2017
Accepted Article published: April 24, 2017
Final Article published: ■■ ▮▮, 0000

COMMUNICATION

Merit badge: Thermoelectric waste heat to electricity conversion requires a high average thermoelectric figure of merit (ZT_{avg}) over the entire working temperature range. $(GeTe)_{80}(AgSbSe_2)_{20}$ (TAGSSe-80), a Pb-free polycrystalline bulk sample, exhibits an ultrahigh ZT_{avg} of 1.4 due to extremely low lattice thermal conductivity in the 300–700 K range.

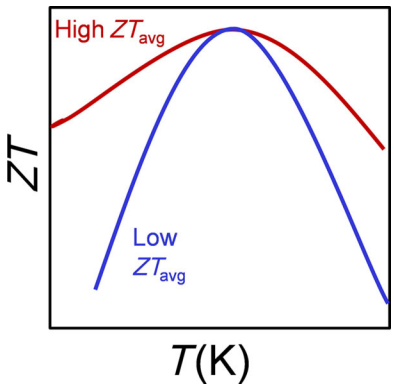

Thermoelectrics

*M. Samanta, S. Roychowdhury, J. Ghatak, S. Perumal, K. Biswas**

■■ – ■■

Ultrahigh Average Thermoelectric Figure of Merit, Low Lattice Thermal Conductivity and Enhanced Microhardness in Nanostructured $(GeTe)_x(AgSbSe_2)_{100-x}$